Desalination and Water Treatment
www.deswater.com

doi: 10.5004/dwt.2020.26255

204 (2020) 306–316
November

Temperature, pH, and Cr(VI) ions sensing with green synthetic carbon dots

Kuan Luo[a], Runmin Huang[a], Jingang Yu[a,b], Xinyu Jiang[a,b,*]

[a]*School of Chemistry and Chemical Engineering, Central South University, Changsha 410083, China, emails: 1752359201@qq.com (K. Luo), 89010456@qq.com (R. Huang), yujg@csu.edu.cn (J. Yu), jiangxinyu@csu.edu.cn (X. Jiang)*
[b]*Key Laboratory of Hunan Province for Water Environment and Agriculture Product Safety, Changsha 410083, China*

Received 15 January 2020; Accepted 13 June 2020

ABSTRACT

In this paper, *Syzygium samarangenses* were utilized to prepare bio-carbon dots via a one-step hydrothermal protocol. Based on the inner filter effect, this fluorescent nanomaterial enables selective detection of Cr^{6+} with a linear range of 10–200 μM and a limit of detection of 7.8 μM through variation in fluorescence. Meanwhile, it also displays that the carbon dots show excellent reversibility and photostability in pH measurements. The intensity of photoluminescence is linear against pH value from 6 to 12 in the buffer solution. In contrast to most of the reported nanomaterials-based pH sensors that rely on the attachment of additional dyes, this carbon-dots-based probe is low in toxicity, easy to synthesize, and free from labels. More importantly, due to a significant fluorescence quenching by temperature-induced aggregation of carbon quantum dots (CQDs), the resultant CQDs have commendable potential as an eminent luminescent thermometer sensor, particularly, the fluorescence intensity (FL intensity) is responsive to temperature and approximately linear in the physiological temperature range from 5°C to 44°C.

Keywords: Bio-carbon dots; Optical temperature sensing; Monitoring of pH; Chromium(VI); Fluorescent probe

1. Introduction

pH plays a vital role in modulating many biological reactions including calcium regulation [1], cell cycle control [2] and apoptosis [3], neurological disorders [4], muscle contraction [5], and tumor growth [6]. Meanwhile, the temperature is a fundamental thermodynamic variable that strongly affects physiological actions and processes. Temperature is also a key parameter to induce some changes in cellular events. For instance, in the process, that consumes ATP (Ca^{2+} ATPase, actinomyosin ATPase, and Na^+/K^+ ATPase) and in the mitochondrial respiratory chain, those actions are exothermic in the forward direction [7]. To date, several promising nanomaterials have been reported for temperature determination/pH sensing, such as scanning probe microscopy, Raman spectroscopy, and fluorescence-based measurements [8–10]. However, among these distinctive methods, fluorescence-based strategies have attracted considerable attention due to their easy operations, simple instruments, and eminent sensitivity [11,12]. Indeed, several fluorescent nanomaterials have been developed for temperature/pH monitoring, such as semiconductor quantum dots, organic dyes, and fluorescent polymers [13–15]. Furthermore, fluorescent nanomaterials have provided a sensor platform useful for temperature/pH sensors in water or biological systems, and especially live cells [16,17]. Even so, their cytotoxicity, poor photostability, and/or tedious probe preparation procedures are problematic, which limits their further application [18,19]. During recent years, nanomaterials-based ratiometric fluorescence pH sensors have been employed to measure pH in living cells, while optical temperature sensing based on luminescent materials is rarely reported [20].

To our knowledge, chromium (Cr) is a common environmental pollutant and widely used in a range of industries,

* Corresponding author.

and exists in two stable oxidation states: Cr(III) and Cr(VI). Among them, Cr(VI)[21,22], possessing greater mobility and carcinogenic properties, is more hazardous to public health compared to Cr(III). In view of the above situation, the monitoring of Cr^{6+} in environmental samples has drawn increasing attention, and the concentration of Cr^{6+} in drinking water is strictly regulated to a lower micromolar level by many nations. In the past few decades, several methods are available for the determination of Cr^{6+} in different sample matrices, including inductively coupled plasma-mass spectrometry (ICP-MS) [23], chromatography [24], voltammetry [25], atomic absorption spectrometry [26], and fluorescence [27,28]. Even though, the reported methods require expensive equipment, complicated sample pretreatment, and highly trained operators. Thus, it is still greatly desirable to develop strategies that are facile and selective for monitoring of Cr^{6+} ions, irrespective of the presence of Cr^{3+}. Due to the distinct advantages of rapid response, facile operation, and excellent sensitivity, the fluorescence-based nanomaterials for the monitoring of Cr^{6+} is a good alternative.

In this work, bio-carbon dots were prepared by utilizing *Syzygium samarangenses* via a one-step hydrothermal protocol. The resultant carbon quantum dots (CQDs) which possessed distinctive optical properties were successfully applied to selectively detect Cr(VI), irrespective of the presence of Cr(III). Meanwhile, the CQDs present an obvious pH-sensitive feature and the intensity of photoluminescence decreases linearly in the pH range from 6 to 12. What's more, as optical temperature sensor, its luminescence intensity linearly decreased within the range from 5°C to 44°C with distinctive sensitivity and marvelous reversibility.

2. Experimental section

2.1. Materials and reagents

Fresh *S. samarangenses* were purchased at a local fruit shop. The phosphate buffer saline (PBS, 0.01 M) was prepared by Beijing Dingguo Changsheng Biotechnology Co., Ltd., (Beijing, China). $CaCl_2$, $Cr_2(SO_4)_3{\cdot}6H_2O$, $Al_2(SO_4)_3$, $K_2Cr_2O_7$, NH_4Cl, $Cu(NO_3)_2$, $MgSO_4$, $Cd(NO_3)_2$, $FeCl_3{\cdot}6H_2O$, $Ni(NO_3)_2$, KI, $Zn(NO_3)_2$, $HgCl_2$, $AgNO_3$, $Pb(NO_3)_2$, NaOH, and HCl were purchased from Sinopharm Chemical Reagent Co., Ltd., (Shanghai, China). All reagents were analytical reagent grade. Ultrapure water with a resistivity of 18.25 MΩ cm^{-1} by a molecular water purification system was used for the preparation of all aqueous solutions.

2.2. Apparatus

LS-55 spectrofluorometer (PerkinElmer, USA), SDC-6 intelligent energy saving thermostat (Ningbo SCIENTZ Biotechnology Co., Ltd., Ningbo, China), pH meter (Mettler Toledo Le438, Switzerland), SCIENTZ-20N vacuum freeze dryer (Ningbo SCIENTZ Biotechnology Co., Ltd., Ningbo, China), Jing Hong Oven, DHJF-8002 quick freezing machine (Zheng Zhou Great Wall Co., Ltd., Zheng Zhou, China). Fluo Time 100 (PicoQuant, Germany), UV-2600 UV-vis spectrophotometer (Shimadzu, Japan), Bruker IFS 66v/S infrared spectrophotometer (Bruker Optics Inc., Billerica, MA, USA), HT7700 transmission electron microscopy (TEM, Hitachi, Japan), PHI 5000C ESCA X-ray photoelectron spectroscopy (XPS, PerkinElmer, USA), Malvern Zetasizer (ZEN 3600, Worcestershire, UK).

2.3. Preparation of bio-carbon

In brief, 10 g of fresh *S. samarangense* and 15 mL of ultrapure water was mixed evenly in the beaker. Then, the mixture was transferred into a 50 mL Teflon-lined autoclave and treated at 180°C for 10 h. After finishing, wait for reactor to cool naturally. The bright brown solution was collected through a 0.22 μm filter membrane and then further purified by dialyzing against ultrapure water using a tubular dialysis membrane (MWCO ~1 kDa) for 48 h. Finally, the purified product solution was dried to a solid powder state through a vacuum freeze dryer.

2.4. Cr(VI) ions sensing

The concentration of CQDs was adjusted to 50 μg mL^{-1}. Aqueous solutions containing 15 different inorganic ions (50 μM, Ca^{2+}, Cr^{3+}, Al^{3+}, Cr^{6+}, NH_4^+, Cu^{2+}, Mg^{2+}, Cd^{2+}, Fe^{3+}, Ni^{2+}, I^-, Zn^{2+}, Hg^{2+}, Ag^+, and Pb^{2+}) were prepared respectively, which were then subjected to fluorescence measurements. To evaluate the detection performance for Cr(VI), in a typical assay, 300 μL of CQDs solution (50 μg mL^{-1} in 0.01 M PBS, pH 7.0) was added to 350 μL quartz cell, and then Cr^{6+} aqueous solutions with different volumes were added to the system. The solutions containing different concentrations of Cr^{6+} (0, 5, 8, 10, 30, 50, 80, 100, 120, 150, 180, 200, 230, 250, 280, and 300 μM) were acquired by diluting with phosphate buffer saline (PBS) (0.01 M, pH 7.0).

2.5. pH sensing

Considering that the FL intensity of quantum dots is affected by temperature, the temperature of the air-conditioned room is locked at 23°C when pH sensing is performed. In detail, a series of fluorescent CQDs solutions with pH ranging systematically from 2 to 12 were prepared with PBS (0.01 M) buffer, and the FL intensity of fluorescent CQDs in different pH values was monitored with a spectrofluorimeter. For the reversibility of the switching operation upon variation of pH, 0.1 M HCl, and 0.1 M NaOH were used to adjust the pH of the CQDs solution from acidic to alkaline and then from alkaline to acidic.

2.6. Temperature sensing

In order to reduce the experimental error as much as possible, the temperature of CQDs aqueous solution is locked at 5°C, 12°C, 17°C, 22°C, 30°C, 38°C, 44°C, 50°C, 56°C, and 60°C by an intelligent energy saving thermostat. Moreover, temperature cycling was carried out to evaluate the reversibility with respect to thermal response of CQDs.

3. Results and discussion

3.1. Characterization of bio-carbon

The synthesis process of bio-carbon was simply described by Fig. 1. The synthetic approach follows the controlling

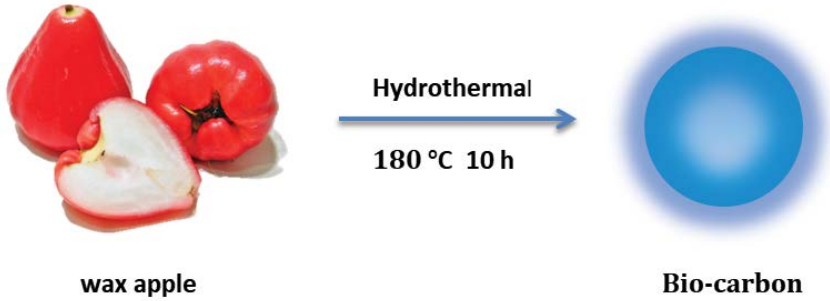

Fig. 1. Scheme for the synthesis of CQDs by *Syzygium samarangense*.

hydrothermal treatment (180°C) of *S. samarangense* for 10 h. The quantum yield (QY) of the as-prepared CQDs in aqueous solution at room temperature is found to be 1.3% using quinine sulfate (0.1 mol L^{-1} H_2SO_4 as solvent; QY = 0.54) as a reference (Fig. S1).

The morphology and structure of the resultant CQDs were investigated by TEM. TEM images (Fig. 2a) show that the as-prepared CQDs appear as spherical particles with an average diameter of 1.9 nm (Fig. 2b).

Fourier transform infrared (FT-IR) spectroscopy was used to determine the surface functional groups of the prepared CQDs. As shown in Fig. 2c, the existence of a broad peak at 3,441.20 cm^{-1} reveals the stretching vibrations of O–H or N–H bond [29]. The peak at 1,635.83 cm^{-1} is attributed to C=O stretching vibration [17]. The peaks at 1,456.02 and 1,199.53 cm^{-1} correspond to the C–N and C=N bonds, respectively [16,17]. Respectively, the 1,400.94 cm^{-1} could be ascribed to the C–H bond [30] and 653.76 cm^{-1} could be assigned to the S–C bond. The absorption peak at 1,135.88 cm^{-1} could be attributed to the stretching vibration of C–O–C [31], and the peak at 1,094.00 cm^{-1} could be identified as C–O group [12]. A highly negative apparent zeta potential value (Fig. 2d) of –20.3 mV, further demonstrates that the CQDs are negatively charged which is obvious for a carboxyl-rich nanoparticle on its periphery [32].

XPS was also carried out to explore the surface composition and chemical state of the as-prepared CQDs. XPS survey spectrum (Fig. 3a) indicated that the CQDs were

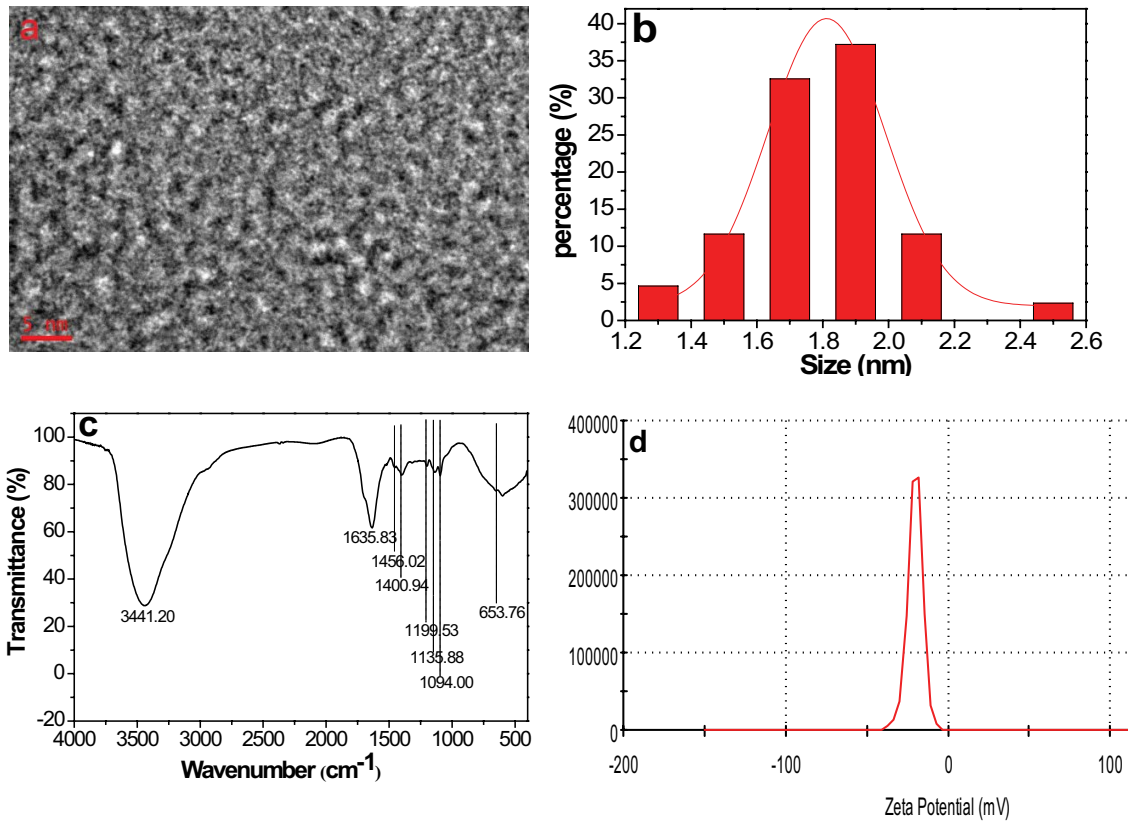

Fig. 2. (a) TEM image of CQDs, (b) size distribution of CQDs, (c) FT-IR spectra of CQDs, and (d) zeta potential of CQDs.

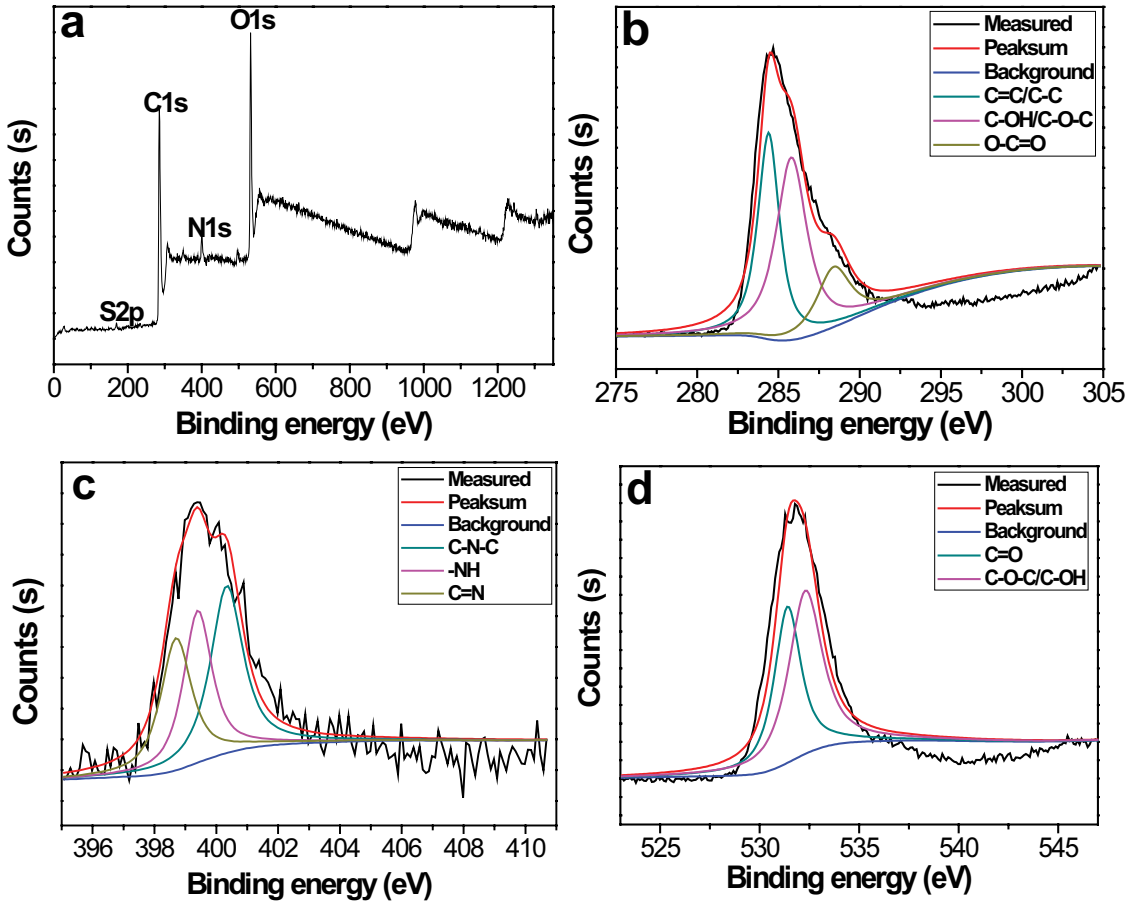

Fig. 3. (a) XPS spectrum of CQDs. High-resolution XPS spectra of C1 s (b), N1 s (c), and O1 s (d).

mainly composed of oxygen (O1s, 531.78 eV), nitrogen (N1s, 399.38 eV), carbon (C1s, 284.68 eV), and sulfur (S2p, 168.78 eV) elements. In detail, the high-resolution XPS spectra for C 1s are divided into three-unit moieties, with the binding energy being 284.4, 285.8, and 288.4 eV (Fig. 3b). They are ascribed as C=C/C–C, C–OH/C–O–C, and O–C=O, respectively [33]. The N 1s spectrum (Fig. 3c) presents the nitrogen signals of C=N at 398.7 eV, –NH at 399.4 eV and C–N–C at 400.4 [30,34]. Two peaks showing at 531.4 and 532.3 eV are assigned to the C=O and C–O–C/C–OH functional groups, respectively [30] (Fig. 3d). The binding energy peaks at 167.5, 168.2, and 168.9 eV reveal that sulfur exists mostly in the form of –C–SO_x – (x = 2, 3, and 4; Fig. S2) [31]. The results of XPS further confirmed the previous FT-IR data. From FT-IR spectrum, XPS, and zeta potential value, it is very clear that the degree of carboxylic acid functionalization is quite high in the as-prepared CQDs.

3.2. Analytical performance for Cr(VI) ions

The fluorescence responses of CQDs upon the addition of different inorganic ions were studied. As shown in Fig. 4a, the FL intensity was the feeblest when Cr^{6+} was introduced to the CQDs composite solution, indicating that CQDs could be utilized to selectively monitor Cr^{6+} in aqueous solution. Fluorescence spectrum of CQDs in the presence of different concentrations of Cr^{6+} under 357 nm excitation is shown in Fig. 4b. The fluorescence intensity of CQDs at around 433 nm decreases gradually with the increase of Cr^{6+} concentration, implying that the addition of Cr^{6+} could effectively quench the fluorescence of CQDs. As shown in Fig. 4c, the linear regression equation (y = –2.2021x + 757.2595) with a correlation coefficient of 0.994 revealed good linearity over the range of 10–200 μM. The limit of detection (LOD) was calculated to be 7.8 μM (LOD = 3σ S^{-1}). Compared to the reported technologies, the developed method showed a wider linear range for the sensing of Cr^{6+} (ESM Table S1).

To evaluate the feasibility of the CQDs for Cr^{6+} detection in the obtained actual water samples, the developed method was applied to detect three real water samples including industrial wastewater, Xiangjiang river of Changsha, and tap water of laboratory. Standard addition experiments were performed with the above three actual water samples to validate this method, and the analytical results are presented in Table 1. The recoveries ranged from 97.4% to 116.3% for the above three water samples, and a relative standard deviation (RSD) of around 8.3% was obtained. Importantly, the results were in good agreement with those obtained from inductively coupled plasma optical emission spectroscopy (ICP-OES).

To explore the sensing mechanism of Cr^{6+}, UV-vis spectra are implemented. As shown in Fig. 5a, the excitation spectrum

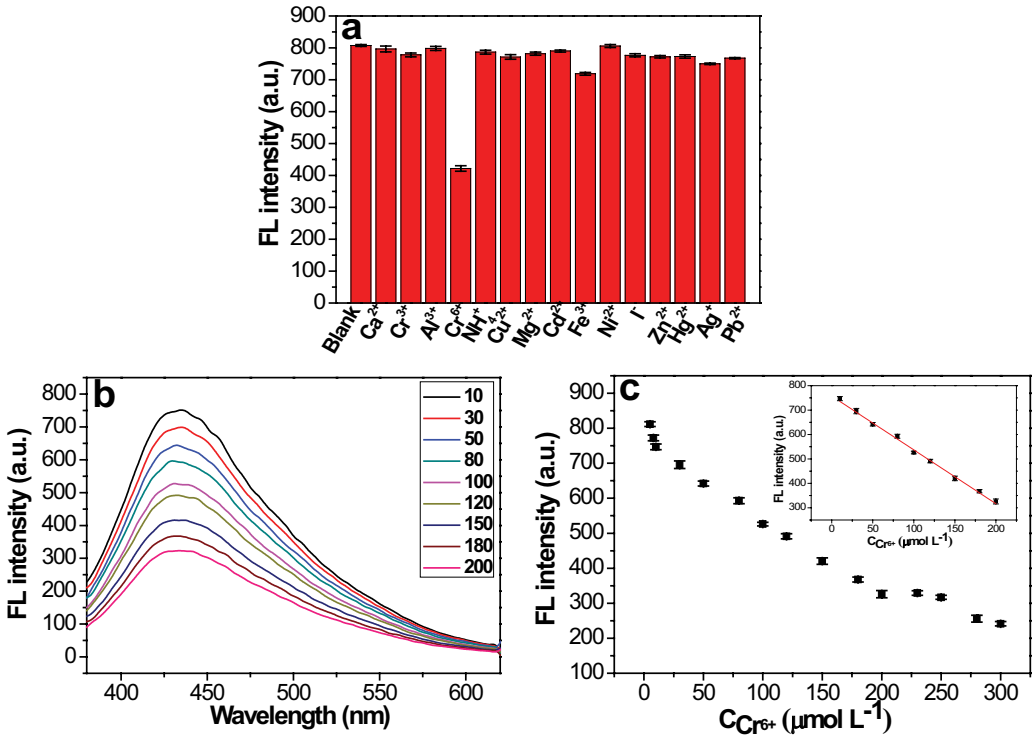

Fig. 4. (a) Selectivity for various metal ions. All competing ion solutions were 50 μM, (b) representative fluorescence emission spectra of CQDs in the presence of increasing Cr^{6+} concentrations (10–200 μM) in 0.01 M PBS at pH 7.0, and (c) relationship between FL intensity and Cr^{6+} from 5 to 300 μM. Inset: a linear plot was obtained in the concentration range of Cr^{6+} from 10 to 200 μM.

Table 1
Cr^{6+} detection in diverse real samples

Sample	No.	Added (μM)	Found[a] (μM)	Recovery (%)	RSD (%) $n = 3$	ICP-OES (μM)
Industrial wastewater	1	0	0	N/A	7.3	0
	2	50	49.12	98.24	5.3	46.01
	3	100	112.8	112.8	6.1	91.68
	4	150	159.0	106.0	3.7	129.7
Xiangjiang river of	1	0	0	N/A	2.9	0
Changsha	2	50	48.70	97.40	4.8	46.03
	3	100	109.7	109.7	4.2	94.13
	4	150	161.9	107.9	7.1	143.2
Tap water of laboratory	1	0	0	N/A	5.4	0
	2	50	58.14	116.3	3.4	45.37
	3	100	107.7	107.7	2.6	88.86
	4	150	147.0	97.98	8.3	142.4

N/A: Not applicable.
[a]Average of three measurements

of CQDs has one band at 357 nm (A), and the emission band of CQDs under the excitation of 357 nm is centered at 433 nm (B); however, Cr^{6+} exhibits broad absorption at 257, 354, and 436 nm (C), respectively, showing a quite precise overlapping with the excitation and emission bands of CQDs. As a consequence, this indicated the quenching could happen by the inner filter effect (IFE) or/and fluorescence resonance energy transfer (FRET) process. Further, as shown in Fig. 5b, the fluorescence decay time of the CQDs is 3.53 ns. The lifetime increased to 3.88 ns with the addition of Cr^{6+} into the solution of CQDs. This small change in lifetime suggests that it is reasonable to exclude FRET as a possible mechanism in Cr^{6+} quenching. What's more, the absorption spectra of the CQDs, CQDs with Cr^{6+}, and Cr^{6+} were examined (Fig. 5c) and there was little difference in the CQDs absorption spectra when Cr^{6+} was added. This confirmed the absence of ground-state

complex formation. Hence, the IFE served as the primary quenching mechanism for CQDs in the presence of Cr^{6+}.

3.3. Analytical performance for pH sensing

The effect of pH on the fluorescence intensity of the CQDs was evaluated and the results are illustrated in Fig. 6. In contrast to the most pH-insensitive CQDs, the as-prepared CQDs have a pH-sensitive feature. Fig. 6a records the gradual decrease of FL intensity in the pH range from 6 to 12. Fig. 6b reveals the fluorescence intensity of CQDs with different pH values, in which the fluorescence intensity of CQDs decreases gradually as the pH ranging from 2 to 12. Obviously, a good linear correlation ($y = -102.6793x + 1{,}326.6689$) within pH 6–12 (Fig. 6b, inset) with a correlation coefficient square (R^2) of 0.995 can be obtained. What's more, it is found that the pH-response of FL intensity is reversible. The FL intensity decreases when pH is tuned from 6 to 12 by adding NaOH solution, and afterward, it increases back to the initial value as pH is changed

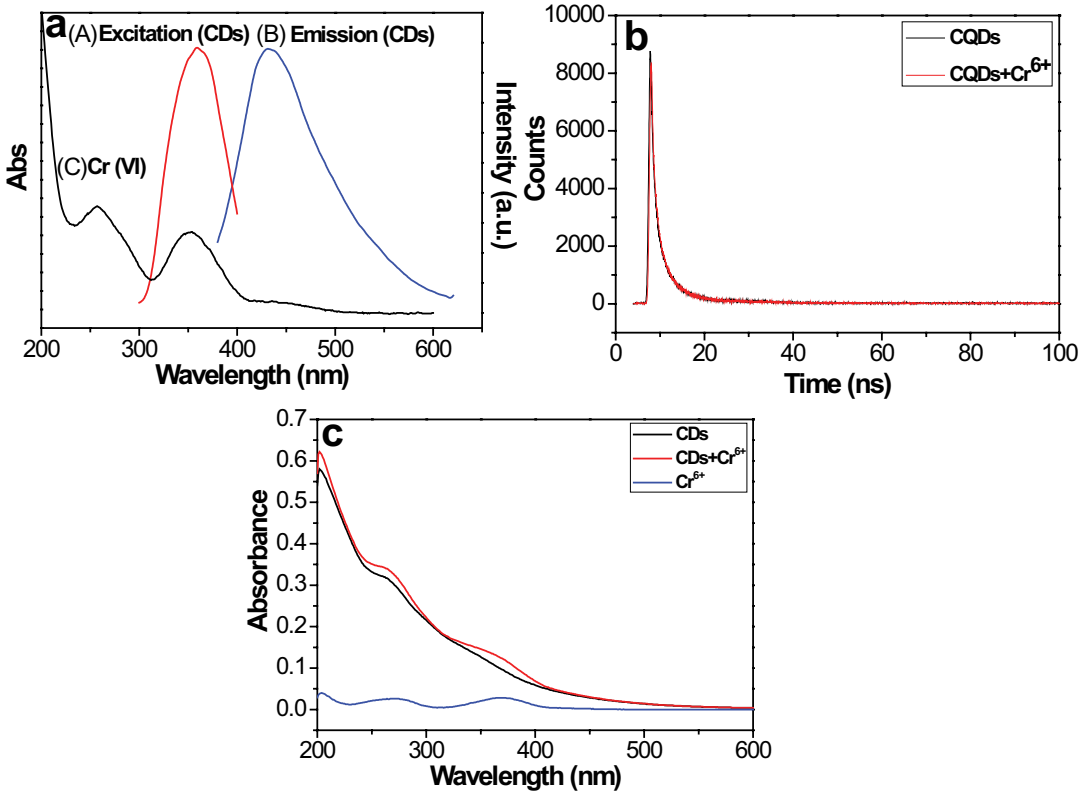

Fig. 5. (a) Fluorescence excitation (A) and emission (B) spectra of CQDs and UV-vis absorption spectrum of Cr^{6+} (C), (b) time-resolved fluorescence decay of CQDs, and CQDs/Cr^{6+}, and (c) UV-vis adsorption for Cr^{6+}, CQDs, and CQDs with Cr^{6+}.

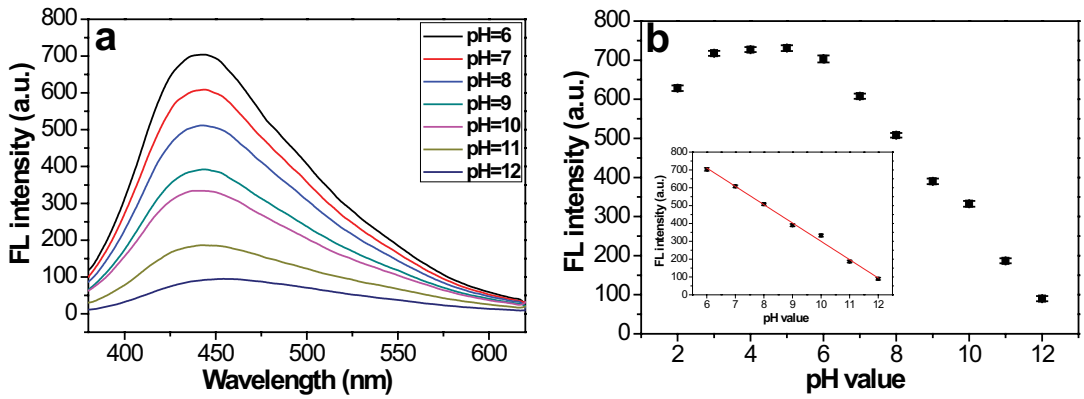

Fig. 6. (a) FL spectra of the CQDs dispersion at different pH values (from 6 to 12) with excitation at 357 nm and (b) FL intensity of the CQDs dispersion at different pH values (from 2 to 12). Inset in (b): plot of the FL intensity at 433 nm against the pH values from 6 to 12.

from 12 to 6 by dropping HCl solution. This process can be repeated several times (Fig. S3). Meanwhile, the color of the CQDs aqueous solution is darkened from light red to yellow (Fig. S4). The above results present that the CQDs are potential as fluorescent and colorimetric sensors for pH monitoring, especially in the physiological pH range. Such a detection method was comparable or superior to other methods in the linear range for the detection of pH (ESM Table S2).

To gain more insight into the origin of the FL behavior, and explain optical responses to change in pH, TEM, and UV-vis spectra are implemented. As shown in Fig. 7a, the resultant CQDs show little change in the UV-vis spectra upon increasing the pH value from 6 to 12. However, the observed change of the FL intensity can be attributed to the formation of larger particles. It is found that the average diameter of CQDs under pH = 10 is 2.3 nm (Fig. 7a), while the average diameter of CQDs under pH = 7 is 1.9 nm (Fig. 2b). Obviously, the increase in diameter of CQDs between pH = 7 and 10 is detected. Correspondingly, the color of the solution changed from light red to yellow as the pH value increased from 6 to 12 (Fig. S4). It could be concluded that the CQDs were dissolved as isolated species in the aqueous under low pH values, on the contrary, the aggregation CQDs appeared with increasing the pH value due to noncovalent molecular interaction, such as hydrogen bond between the carboxyl groups [35]. Thus, pH-induced aggregation of the resultant CQDs gives rise to a distinct fluorescence quenching at high pH values.

3.4. Analytical performance for temperature sensing

In temperature range from 5°C to 60°C, the fluorescence of CQDs was also investigated to study the influence of temperature (Fig. 8). Fig. 8a shows the significant temperature dependence of emission spectra of the resultant CQDs. The FL intensity decreases by 36.8% upon raising the temperature from 5°C to 60°C. As shown in Fig. 8b, with increasing the temperature from 5°C to 44°C, the FL intensity of the as-prepared CQDs changes close to linearly. A nice linear correlation (y = –5.6613x + 646.8131) over the range from 5°C to 44°C with a correlation coefficient square (R^2) of 0.989 can be obtained. Given this temperature range is larger than the physiological temperature, which suggests as-prepared CQDs have promising application *in vivo* temperature sensing. To verify

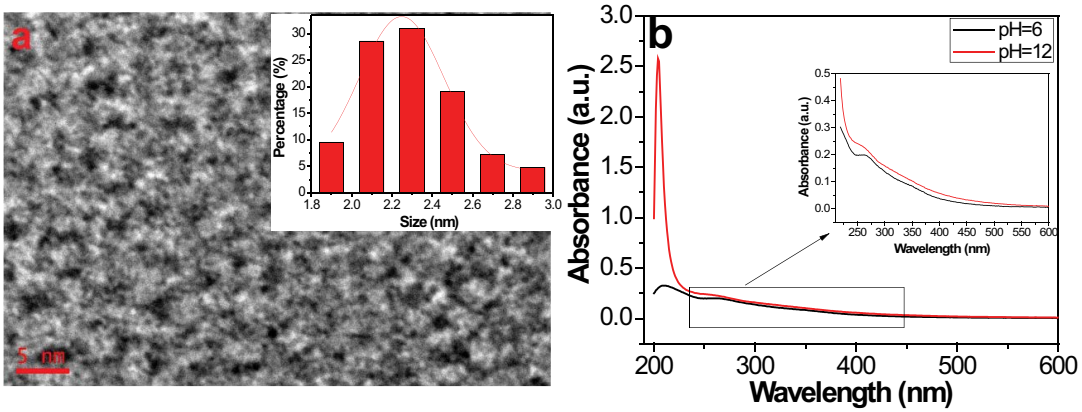

Fig. 7. (a) TEM image of CQDs in an aqueous solution of pH = 10 at room temperature and the size increases up to 2.3 nm and (b) UV-vis absorption spectra of CQDs in aqueous solution under pH = 6 and 12.

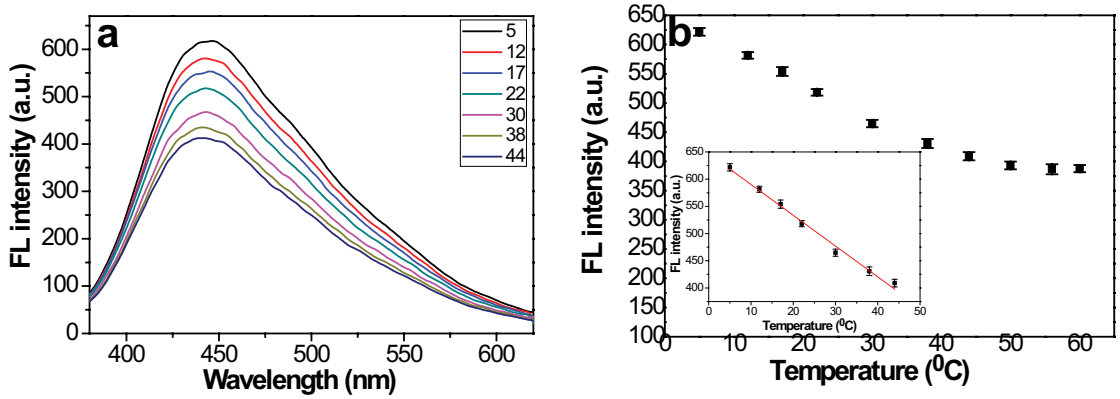

Fig. 8. (a) Fluorescence emission spectra (excitation 357 nm) for various temperatures in the range 5°C–44°C (top to bottom) and (b) intensity at 433 nm is plotted vs. temperature.

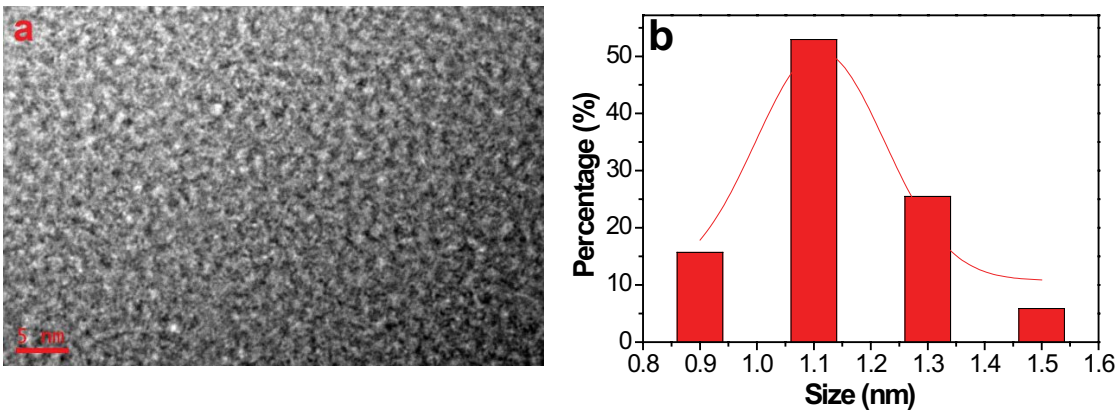

Fig. 9. (a) TEM image of CQDs in an aqueous solution of pH = 7 at 5°C and (b) size distribution of CQDs at 5°C.

the reversibility and restorability of the CQDs fluorescence, the as-prepared CQDs were subjected to temperature cycling between 5°C and 60°C. According to Fig. S5, it was obvious that the fluorescence intensity decreased at a higher temperature and was recovered when the temperature back to 5°C. As a consequence, the CQDs showed noticeable reversibility and restorability whenever the temperature changed. In other words, the temperature (5°C–60°C) cannot result in perpetual destruction on the surface fluorescent structure of the resultant CQDs.

As showed in Fig. 9, TEM was used to study the temperature-responsive FL behavior of CQDs. As shown in Fig. 9a, the size of CQDs has been significantly reduced at 5°C compared with room temperature. It is found that the average diameter of CQDs at 5°C decreased down to 1.1 nm (Fig. 9b), while the average diameter of CQDs at room temperature is 1.9 nm (Fig. 2b). Thus, increasing the temperature, the aggregation of as-prepared CQDs occurred which caused the significant fluorescence quenching.

4. Conclusions

In summary, the CQDs are synthetized by *S. samarangense* via a one-step hydrothermal protocol. Further, the chemical structure and PL mechanism are investigated in detail. With this strategy, we have manifested a simple, rapid, and low-cost on–off fluorescent approach for monitoring of Cr^{6+} using CQDs as a fluorescent nanomaterial based on the IFE. Besides, the fluorescence nanomaterial shows a reversible and sensitive response to pH, especially linear physiological pH dependence for monitoring pH 6–12. Remarkably, the obtained CQDs as a reliable temperature sensor display fascinating temperature-dependent fluorescence with an excellent linear response from 5°C to 44°C. As a consequence, the prepared CQDs have great potential as a novel optical temperature sensor and pH sensor which makes the as-prepared CQDs be a promising candidate in cellular temperature/pH sensing.

Acknowledgments

We gratefully acknowledge the National Natural Science Foundation of China (No. 21571191 and No. 51674292) and Key Laboratory of Hunan Province for Water Environment and Agriculture Product Safety (2018TP1003).

References

[1] A.J. Janecki, M.H. Montrose, P. Zimniak, A. Zweibaum, C.M. Tse, S. Khurana, M. Donowitz, Subcellular redistribution is involved in acute regulation of the brush border Na^+/H^+ exchanger isoform 3 in human colon adenocarcinoma cell line caco-2, J. Biol. Chem., 273 (1998) 8790–8798.
[2] M. Oslo, Regulation of intracellular pH in eukaryotic cells, Biochem. J., 250 (1988) 1–8.
[3] R.T. Kennedy, L. Huang, C.A. Aspinwall, Extracellular pH is required for rapid release of insulin from Zn–insulin precipitates in β-cell secretory vesicles during exocytosis, J. Am. Chem. Soc., 118 (1996) 1795–1796.
[4] A.M. Dennis, W.J. Rhee, D. Sotto, S.N. Dublin, G. Bao, Quantum dot-fluorescent protein FRET probes for sensing intracellular pH, ACS Nano, 6 (2012) 2917–2924.
[5] E.R. Chin, D.G. Allen, The contribution of pH-dependent mechanisms to fatigue at different intensities in mammalian single muscle fibres, J. Physiol., 512 (1998) 831–840.
[6] X. Zhang, Y. Lin, R.J. Gillies, Tumor pH and its measurement, J. Nucl. Med., 51 (2010) 1167–1170.
[7] B.B. Lowell, B.M. Spiegelman, Towards a molecular understanding of adaptive thermogenesis, Nature, 404 (2000) 652–660.
[8] S.H. Kim, J. Noh, M.K. Jeon, K.W. Kim, L.P. Lee, S.I. Woo, Micro-Raman thermometry for measuring the temperature distribution inside the microchannel of a polymerase chain reaction chip, J. Micromech. Microeng., 16 (2006) 526–530.
[9] F. Vetrone, R. Naccache, A. Zamarron, A. Juarranz de la Fuente, F. Sanz-Rodriguez, L. Martinez Maestro, E. Martin Rodriguez, D. Jaque, J. Garcia Sole, J.A. Capobianco, Temperature sensing using fluorescent nanothermometers, ACS Nano, 4 (2010) 3254–3258.
[10] B. Li, H. Ma, B. Zhang, J. Qian, T. Cao, H. Feng, W. Li, Y. Dong, W. Qin, Dually emitting carbon dots as fluorescent probes for ratiometric fluorescent sensing of pH values, mercury(II), chloride and Cr(VI) via different mechanisms, Microchim. Acta, 186 (2019) 341–351.
[11] X. Cui, Y. Wang, J. Liu, Q. Yang, B. Zhang, Y. Gao, Y. Wang, G. Lu, Dual functional N- and S-co-doped carbon dots as the sensor for temperature and Fe^{3+} ions, Sens. Actuators, B, 242 (2017) 1272–1280.
[12] Y. Hu, J. Yang, J. Tian, L. Jia, J.-S. Yu, Waste frying oil as a precursor for one-step synthesis of sulfur-doped carbon dots with pH-sensitive photoluminescence, Carbon, 77 (2014) 775–782.
[13] Y. Jiang, X. Yang, C. Ma, C. Wang, H. Li, F. Dong, X. Zhai, K. Yu, Q. Lin, B. Yang, Photoluminescent smart hydrogels

with reversible and linear thermoresponses, Small, 6 (2010) 2673–2677.
[14] E.J. McLaurin, L.R. Bradshaw, D.R. Gamelin, Dual-emitting nanoscale temperature sensors, Chem. Mater., 25 (2013) 1283–1292.
[15] D. Zhou, M. Lin, X. Liu, J. Li, Z. Chen, D. Yao, H. Sun, H. Zhang, B. Yang, Conducting the temperature-dependent conformational change of macrocyclic compounds to the lattice dilation of quantum dots for achieving an ultrasensitive nanothermometer, ACS Nano, 7 (2013) 2273–2283.
[16] J. Shangguan, D. He, X. He, K. Wang, F. Xu, J. Liu, J. Tang, X. Yang, J. Huang, Label-free carbon-dots-based ratiometric fluorescence pH nanoprobes for intracellular pH sensing, Anal. Chem., 88 (2016) 7837–7843.
[17] W. Shi, F. Guo, M. Han, S. Yuan, W. Guan, H. Li, H. Huang, Y. Liu, Z. Kang, N,S co-doped carbon dots as a stable bio-imaging probe for detection of intracellular temperature and tetracycline, J. Mater. Chem. B, 5 (2017) 3293–3299.
[18] C.D. Brites, P.P. Lima, N.J. Silva, A. Millan, V.S. Amaral, F. Palacio, L.D. Carlos, Thermometry at the nanoscale, Nanoscale, 4 (2012) 4799–4829.
[19] D. Jaque, F. Vetrone, Luminescence nanothermometry, Nanoscale, 4 (2012) 4301–4326.
[20] H. Nie, M. Li, Q. Li, S. Liang, Y. Tan, L. Sheng, W. Shi, S.X.-A. Zhang, Carbon dots with continuously tunable full-color emission and their application in ratiometric pH sensing, Chem. Mater., 26 (2014) 3104–3112.
[21] A. Baral, R.D. Engelken, Chromium-based regulations and greening in metal finishing industries in the USA, Environ. Sci. Policy, 5 (2002) 121–133.
[22] A. Zhitkovich, Chromium in drinking water: sources, metabolism, and cancer risks, Chem. Res. Toxicol., 24 (2011) 1617–1629.
[23] W. Cieslak, K. Pap, D.R. Bunch, E. Reineks, R. Jackson, R. Steinle, S. Wang, Highly sensitive measurement of whole blood chromium by inductively coupled plasma mass spectrometry, Clin. Biochem., 46 (2013) 266–270.
[24] V. Arancibia, M. Valderrama, K. Silva, T. Tapia, Determination of chromium in urine samples by complexation–supercritical fluid extraction and liquid or gas chromatography, J. Chromatogr. B, 785 (2003) 303–309.
[25] S. Abbasi, A. Bahiraei, Ultra trace quantification of chromium(VI) in food and water samples by highly sensitive catalytic adsorptive stripping voltammetry with rubeanic acid, Food Chem., 133 (2012) 1075–1080.
[26] A.N. Anthemidis, G.A. Zachariadis, J.-S. Kougoulis, J.A. Stratis, Flame atomic absorption spectrometric determination of chromium(VI) by on-line preconcentration system using a PTFE packed column, Talanta, 57 (2002) 15–22.
[27] X. Song, H. Sun, S. Yang, S. Zhao, F. Liao, Synthesis of photoluminescent o-phenylenediamine–m-phenylenediamine copolymer nanospheres: an effective fluorescent sensing platform for selective and sensitive detection of chromium(VI) ion, J. Lumin., 169 (2016) 186–190.
[28] K.H. Lu, J.H. Lin, C.Y. Lin, C.F. Chen, Y.C. Yeh, A fluorometric paper test for chromium(VI) based on the use of N-doped carbon dots, Microchim. Acta, 186 (2019) 227–234.
[29] K. Luo, X.Y. Jiang, Fluorescent carbon quantum dots with Fe(III/II) irons as bridge for the detection of ascorbic acid and H_2O_2, J. Fluoresc., 29 (2019) 769–777.
[30] S. Liao, X. Zhao, F. Zhu, M. Chen, Z. Wu, X. Song, H. Yang, X. Chen, Novel S,N-doped carbon quantum dot-based "off-on" fluorescent sensor for silver ion and cysteine, Talanta, 180 (2018) 300–308.
[31] C. Wang, C. Wang, P. Xu, A. Li, Y. Chen, K. Zhuo, Synthesis of cellulose-derived carbon dots using acidic ionic liquid as a catalyst and its application for detection of Hg^{2+}, J. Mater. Sci., 51 (2015) 861–867.
[32] V. Ramanan, S.K. Thiyagarajan, K. Raji, R. Suresh, R. Sekar, P. Ramamurthy, Outright green synthesis of fluorescent carbon dots from eutrophic algal blooms for *in vitro* imaging, ACS Sustainable Chem. Eng., 4 (2016) 4724–4731.
[33] C. Wang, Z. Xu, H. Cheng, H. Lin, M.G. Humphrey, C. Zhang, A hydrothermal route to water-stable luminescent carbon dots as nanosensors for pH and temperature, Carbon, 82 (2015) 87–95.
[34] S. Liao, F. Zhu, X. Zhao, H. Yang, X. Chen, A reusable P,N-doped carbon quantum dot fluorescent sensor for cobalt ion, Sens. Actuators, B, 260 (2018) 156–164.
[35] X. Jia, X. Yang, J. Li, D. Li, E. Wang, Stable Cu nanoclusters: from an aggregation-induced emission mechanism to biosensing and catalytic applications, Chem. Commun., 50 (2014) 237–239.

Supplementary information

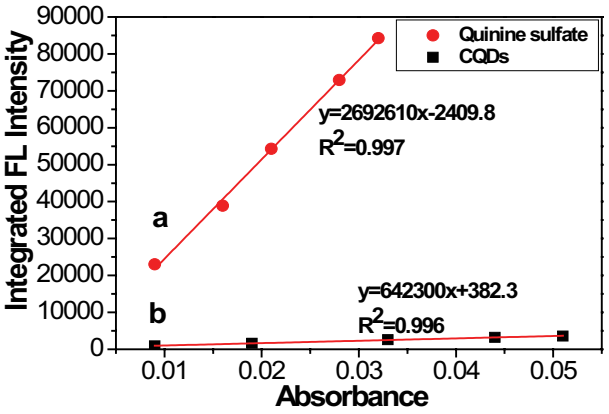

Fig. S1. Linear plots for quinine sulfate (a) and CQDs (b), respectively. The gradient for each sample was proportional to its fluorescence quantum yield.

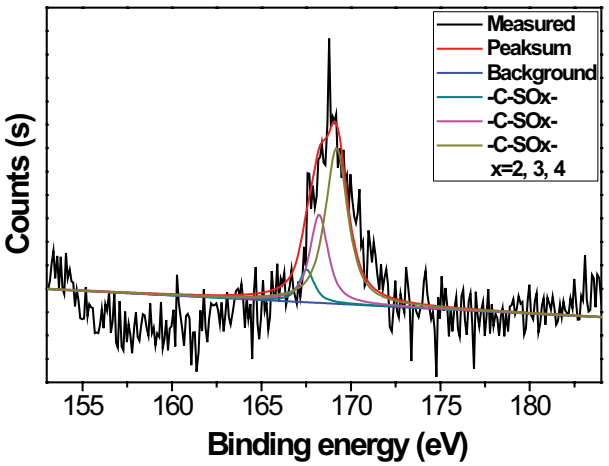

Fig. S2. XPS spectrum of CQDs with the high-resolution XPS spectra of S2p.

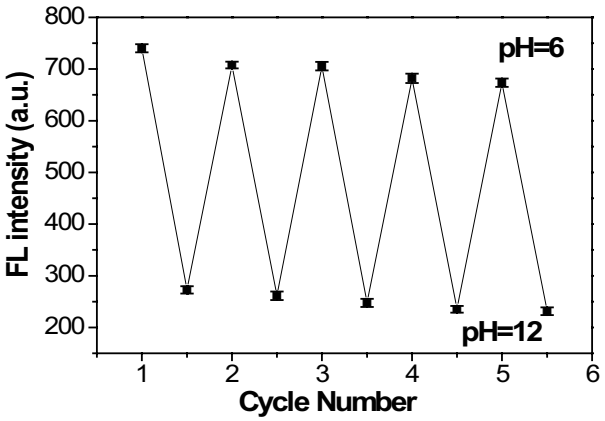

Fig. S3. Reversible pH-response of the FL behavior of the CQDs measured by tuning pH from 6 to 12 and then from 12 to 6.

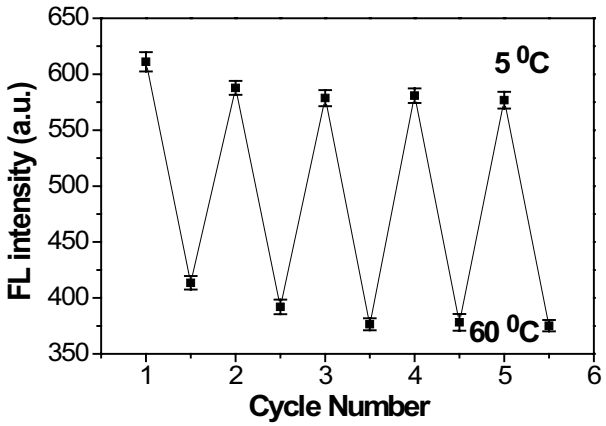

Fig. S5. FL intensity upon the cyclic switching of CQDs under alternating conditions of 5°C and 60°C.

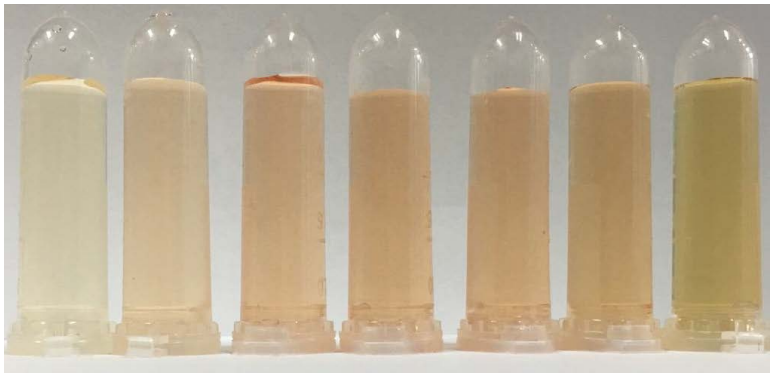

Fig. S4. Photographs of CQDs aqueous solution with the increase of pH value from 6 to 12 under room light.

Table S1
Comparison of detection performance of different fluorescent probes for Cr^{6+} detection

Detection probes	Detection mechanism	Detection limit	Linear range	Reference
GSH@CDs-Cu NCs	Fluorescence quenching	0.9 μM	2–40 μM	[1]
CdTe-CQDs	Fluorescence quenching	0.06 μM	2.5–40 μM	[2]
N-CQDs	Fluorescence quenching	0.25 μM	2–40 μM	[3]
MOF	Fluorescence quenching	3.8 μM	4–40 μM	[4]
N-CQDs	Fluorescence quenching	1.3 μM	5–50 μM	[5]
CQDs	Fluorescence quenching	7.8 μM	10–200 μM	This work

Table S2
Comparison of detection performance of different fluorescent probes for pH detection

Detection probes	Linear range	Reference
Graphene oxide nanosheets (GO)	4.0–8.0	[6]
FITC-modified silicon nanodots	5.4–7.7	[7]
CQDs	5.2–8.8	[8]
CQDs	5.0–8.0	[9]
CQDs	4.0–8.0	[10]
CQDs	6.0–12.0	This work

References

[1] H.Y. Bai, Z.Q. Tu, Y.T. Liu, Q.X. Tai, Z.K. Guo, S.Y. Liu, Dual-emission carbon dots-stabilized copper nanoclusters for ratiometric and visual detection of $Cr_2O_7^{2-}$ ions and Cd^{2+} ions, J. Hazard. Mater., 386 (2020) 121654–121661.

[2] Y. Hu, J.P. Zhang, G. Li, H.W. Xing, M.H. Wu, Highly sensitive fluorescent determination of chromium(VI) by the encapsulation of cadmium telluride quantum dots (CdTe QDs) into zeolitic imidazolate framework-8 (ZIF-8), Anal. Lett., 53 (2020) 1639–1653.

[3] B.G. Wang, Y. Lin, H. Tan, M. Luo, S.S. Dai, H.S. Lu, Z.Y. Huang, One-pot synthesis of N-doped carbon dots by pyrolyzing the gel composed of ethanolamine and 1-carboxyethyl-3-methylimidazolium chloride and their selective fluorescence sensing for Cr(VI) ions, Analyst, 143 (2018) 1906–1915.

[4] T.Y. Xu, J.M. Li, Y.H. Han, A new 3D four-fold interpenetrated dia-like luminescent Zn(II)-based metal–organic framework: the sensitive detection of Fe^{3+}, $Cr_2O_7^{2-}$, and CrO_4^{2-} in water, and nitrobenzene in ethanol, New J. Chem., 44 (2020) 4011–4022.

[5] K.H. Lu, J.H. Liu, C.Y. Lin, C.F. Chen, Y.C. Yeh, A fluorometric paper test for chromium(VI) based on the use of N-doped carbon dots, Microchim. Acta, 186 (2019) 227–233.

[6] J.L. Chen, X.P. Yan, Ionic strength and pH reversible response of visible and near-infrared fluorescence of graphene oxide nanosheets for monitoring the extracellular pH, Chem. Commun., 47 (2011) 3135–3137.

[7] Y.A. Zhang, D.J. Hou, X.L. Yu, Facile preparation of FITC-modified silicon nanodots for ratiometric pH sensing and imaging, Spectrochim. Acta, Part A, 234 (2020) 118276–118282.

[8] D.G. He, X.X. He, K.M. Wang, F.Z. Xu, Label-free carbon-dots-based ratiometric fluorescence pH nanoprobes for intracellular pH sensing, Anal. Chem., 88 (2016) 7837–7843.

[9] H. Nie, M.J. Li, Q.S. Li, S.J. Lian, Y.Y. Tan, L. Sheng, W. Shi, Carbon dots with continuously tunable full-color emission and their application in ratiometric pH sensing, Chem. Mater., 26 (2014) 3104–3112.

[10] X.F. Jia, J. Li, E.K. Wang, One-pot green synthesis of optically pH-sensitive carbon dots with upconversion luminescence, Nanoscale, 4 (2012) 5572–5575.